ORIGINAL ARTICLE

The effect of RFSSW parameters on load capacity of EN AW-6082-T6 aluminum alloy and AlCu bimetallic joints

Andrzej Kubit[1] · Koen Faes[2] · Tomasz Trzepieciński[1] · Krzysztof Żaba[3] · Ľuboš Kaščák[4]

Abstract

This paper presents research into the creation of refill friction stir spot welding (RFSSW) single-lap joints of 6082-T6 aluminum alloy and roll-bonded AlCu bimetallic sheet. The latter sheet comprises aluminum EN AW-1050A and electrolytic copper M1E in Z6 temper condition (after rolling) and with a 1:1 ratio of the Cu:Al layers. The welding parameters involved a variable plunge depth and welding time. The mechanical properties of the joints were determined in tensile/shear tests. The highest average value of the load capacity of the joint was observed in joints made with a tool plunge depth $d_t = 2.6$ mm and total welding time $t_w = 4$ s. The load capacity for this variant was an average of 5986.75 N with standard deviation SD = 166.15 N. A plug-type fracture on the aluminum layer of the bimetallic sheet was observed in RFSSW joints produced with a plunge depth of 2.6 mm. Increasing the tool rotational speed and thus generating heat resulted in a plug-type fracture on the upper sheet (aluminum alloy). In the case of joints produced with a plunge depth of 2 mm equal to the thickness of the upper sheet, the type of fracture mode with both welding times was found to be nugget debonding.

Keywords Aluminum alloy · AlCu bimetallic sheet · Load capacity · RFSSW · Welded joint

1 Introduction

Bimetal is composed of two metals that are permanently connected to each other in terms of their physical and chemical properties [1]. Copper and aluminum bimetal is called cupal (cuprum and aluminum) and is usually manufactured in the form of rolled products (sheets, strips). These are used for inserts when connecting power cables, as well as for high-frequency tracks. AlCu bimetallic sheet is often used for the production of washers, which are necessary to connect copper and aluminum devices [2–4]. Due to the connections made with the use of cupal washers, the phenomenon of the formation of cells at the AlCu interface is eliminated,

which means that they prevent the formation of electro-chemical corrosion [5]. The use of such sheets is possible thanks to the composite properties of the materials that make them up. Copper is responsible for good conductivity and corrosion resistance [6–8]. The choice of AlCu bimetallic sheet is largely influenced by economic factors. The use of aluminum significantly reduces the production costs of such material, compared to the use of pure copper [9, 10].

Bimetallic materials with composite properties can be obtained in many ways, such as twin roll casting, explosive welding, composite rolling, or casting. Each of the above-mentioned methods faces the technological challenge of creating a passivation layer on a copper sheet, one of the input materials [11, 12]. This layer should be mechanically removed and the joining process of copper and aluminum sheets should be rapidly commenced, otherwise this layer may reappear, thus weakening the connection between the two sheets [10]. The strength of the layer connecting the two metals is largely responsible for the quality of such a product. For this reason, tests of their technological and mechanical properties are used on bimetallic sheets [13]. In the case of bimetallic plates obtained by a rolling process, the pre-material has to be hardened by heat treatment in the form of annealing. Such an operation will ensure

✉ Andrzej Kubit
akubit@prz.edu.pl

1   Department of Manufacturing and Production Engineering, Rzeszow University of Technology, Rzeszow, Poland

2   Belgian Welding Institute, Ghent, Belgium

3   Department of Non-Ferrous Metals, AGH University of Science and Technology, Krakow, Poland

4   Department of Technology, Materials and Computer Supported Production, Technical University of Košice, Košice, Slovakia

that plastic properties that are appropriate and necessary for forming by rolling are obtained [13].

The demand for bimetallic sheet products is still growing due to their properties. The combination of different materials into a bimetal allows the use of the properties of both metals [14]. It should be noted that products that are a combination of copper and aluminum are in quite high demand. They are used for the production of, among other items, overhead cable connectors and bimetallic terminals in the electrical, energy, and electronic industries. There are several methods used for joining bimetallic sheets, for example, surfacing, pack rolling, explosive cladding, or friction welding.

Friction stir welding (FSW) of Al–Cu has previously been studied by other authors, focusing mainly on the effects of basic process parameters such as tool feed rate, spindle speed, vertical thrust force, and plunge depth [15]. The material flow in dissimilar FSW of thin Al and Cu sheets was investigated by Galvao et al. [16]. They noted a great difference in the material flow depending on which material was placed on the advancing side. Bhattacharya et al. [17] investigated the material flow in AlCu friction stir butt-welded joints. According to the authors, the classic FSW flow model is that aluminum on the retreating side flows toward the advancing Cu, which flows downstream first and then up again. The morphology of the FSW joint usually consists of two or more intermetallic compound (IMC) phases and the formation is influenced by process parameters as found by Liu et al. [18] and Galvão et al. [19]. The most commonly formed IMCs are $CuAl_2$ (Θ) and Cu_9Al_4 (γ_1) [20, 21]. Manickam et al. [22] employed friction stir spot welding (FSSW) to join dissimilar metals consisting of commercial copper alloy and 6061-T6 aluminum alloy. The effect of plunge rate, tool rotational speed, and dwell time on the maximum shear fracture load was considered. It was found that the continuous formation of IMCs such as η_2-CuAl in the Al zone and γ_2-Cu_9Al_4 in the Cu zone may enhance the shear fracture load. Friction stir spot welding was also used to join aluminum to steel, aluminum to aluminum [22, 23], aluminum to titanium [24], and aluminum to magnesium [25, 26]. Joining of dissimilar alloys using conventional fusion techniques produces joints of unacceptable soundness due to complex weld pool shapes, high residual stresses, cracking and low strength, microporosity, and the formation of brittle IMCs, leading to poor formability or inferior mechanical properties [24]. The advantages of friction welding in a solid state include the possibility of joining materials that differ significantly in physical properties, the possibility of joining sheets with a significant difference in thickness, the high repeatability of welding results, and the possibility of management and quality control during the welding cycle [27].

Refill friction stir spot welding (RFSSW) has been developing dynamically in recent years. This method uses a three-piece non-consumable tool consisting of stationary clamping, and a movable sleeve and pin, which, by performing an alternating plunge movement, enable better mixing of the materials to be joined in the nugget zone. In addition, it is possible to obtain a craterless weld and the RFSSW technique can be applied to weld plates of different thicknesses. Chai et al. [28] used the RFSSW technique to join dissimilar Al/Mg alloys and to analyze the effect of tool plunge depth on the mechanical properties of the joints. The IMC at the pin-affected zone was thicker than that at the sleeve-affected zone because of its flow characteristics. The IMCs in the sleeve-affected zone were thinner than those in the pin-affected zone because of their flow characteristics. Zou et al. [29] welded 2-mm-thick EN AW-2219-O aluminum alloy plates to EN AW-2219-C10S plates of various thicknesses (4–14 mm) via RFSSW. Compressive and tensile stresses were mainly distributed along the direction of the force on both sides of the weld nugget. However, shear stresses were distributed in a direction perpendicular to the external force. Liu et al. [30] used RFSSW to join EN AW-6061-T6 and EN AW-7075-T6 aluminum alloys. They found that with increasing sleeve plunge depth, better material mixing occurs between the upper and lower sheets. Furthermore, no defects are observed when using 6061-T6 aluminum alloy as the upper sheet. Fritsche et al. [31] used the RFSSW technique to join AlSi10Mg processed by laser powder bed fusion with EN AW-7075-T6 aluminum alloy. Various tool rotational speeds at constant plunge depth and welding time were considered. It was found that hook height and joint integrity are the key parameters influencing the load capacity of the joints. RFSSW is commonly used to join various grades of aluminum alloys used in the aerospace and automotive industries [32, 33]. Takeoka et al. [34] developed scrubbing RFSSW (sc-RFSSW) to join noncoated mild steel and aluminum alloy. It was found that sc-RFSSW provides a higher maximum joint load than that of conventional FSSW.

The demand for high-strength bimetallic joints, in particular, AlCu joints for electrotechnical purposes, is growing intensively due to the development of electric motorization [35]. Especially in automotive applications, it is extremely important to ensure not only high static strength of joints but above all fatigue life and dynamic strength [36–38]. The above-mentioned problems are inherent in the welding of various materials together. Growing requirements from electric car manufacturers led the authors of this work to a new concept of making structural joints of aluminum alloys with copper used for electrotechnical purposes. Since the production of AlCu bimetallic sheets is well developed in terms of technology [10, 39], it was decided to join such bimetals from the side of the EN AW-1050A aluminum alloy

layer with an EN AW-6082-T6 aluminum alloy, which is supposed to ensure high quality of the joint, including its good fatigue life. On the other hand, electrical copper joints in such a joined structure are assumed to be welded directly to the Cu layer of the bimetallic sheet. Ultrasonic welding is currently a promising technology for the production of such joints [35]. This assumption solves a number of problems related to the production of joints between dissimilar materials, and for economic reasons, it is the right solution for the automotive industry.

The feasibility of using RFSSW technology to join similar and dissimilar alloys has already been confirmed. However, there are no systematic studies in the literature investigating the joining of EN AW-6082-T6 aluminum alloy with bimetallic sheets. This study reports previously unavailable results concerning the mechanical properties of joints between dissimilar materials produced by the RFSSW of EN AW-6082-T6 aluminum alloy sheet and CuAl bimetallic sheet. A wide range of values of tool plunge depth in combination with welding times were considered to ensure maximum joint load capacity and to determine the type of fracture mode.

2 Materials and methods

2.1 Material

This paper considers the formation of RFSSW joints between EN AW-6082-T6 aluminum alloy and AlCu bimetallic sheets. AlCu bimetallic strips in Z6 temper condition (after rolling) and a 1:1 ratio of Cu:Al layers were used in this study. The sheets were produced by the roll bonding method in industrial conditions in Walcownia Dziedzice S.A. The input materials for the production of AlCu bimetallic sheets were sheets of technical grade aluminum EN AW-1050A and of electrolytic copper M1E. The chemical composition of AlCu bimetallic sheet material is shown in Table 1.

2.2 RFSSW procedure

Harms & Wende GmbH produced RFSSW-bonded single-lap joints between AlCu bimetallic sheets and EN
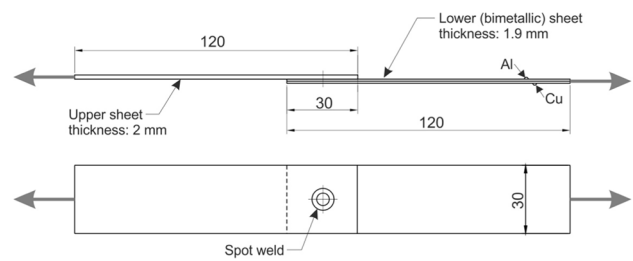

Fig. 1 Dimensions (in mm) of the specimen for tensile/shear testing

AW-6082-T6 aluminum alloy sheet (Fig. 1) using an RPS100 spot welder. The RFSSW welding tool consists of three components [40]: a pin with a diameter of 5.2 mm, a sleeve with an external diameter of 9 mm, and a clamping ring. The detailed procedure of the refill friction stir spot welding process can be found in previous papers by the authors [32, 40]. The welding procedure generally consists of four steps: touchdown, plunging, refilling, and tool retraction.

The parameters of the RFSSW process were selected based on preliminary tests, on the basis of which it was found that the conditions ensuring the formation of the correct joint are obtained with equal values of plunge time and retraction time, as well as with a dwell time of 0 s. It was determined that the total welding time (dwell time and retraction time) for the joint considered should be at least $t_w = 4$ s. With a lower value of welding time, the material plasticization process does not take place to a sufficient degree to produce the correct joint. On the other hand, a welding time with a value greater than $t_w = 6$ s leads to excessive growth of the heat-affected zone (HAZ), which in turn weakens the materials to be joined. Moreover, a long welding time is economically disadvantageous. Therefore, two values of welding time were considered, i.e., 4 s, which variant was called "short welding time"—ST, and 6 s, which was referred to as "long welding time"—LT.

Plunge depth was a variable parameter. Due to the specific features of the welding process of bimetallic sheets, an option was considered in which the tool was only plunged into the interface between the joined sheets, assuming that the joint would be formed thanks to thermoplastic processes as schematically shown in Fig. 2a. In this variant, it was assumed that the thermo-mechanically affected zone (TMAZ) did not interfere with the copper layer of

Table 1 The chemical composition of AlCu bimetallic sheet

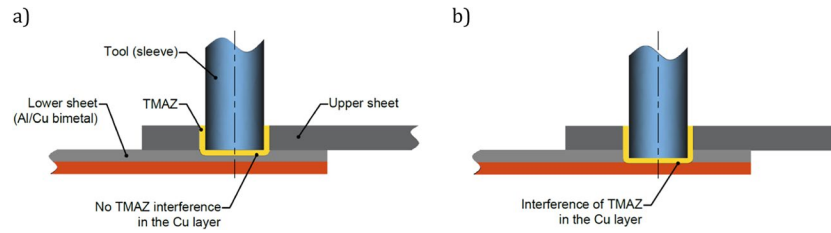| Side	Aluminum EN AW-1050A								
Element	Al	Mg	Mn	Fe	Si	Cu	Zn	Ti	Rest
% wt	99.43	0.025	0.027	0.23	0.17	0.028	0.033	0.029	0.028
Side	Copper M1E								
Element	Cu	Bi	O	Pb	Rest				
% wt	99.93	0.0004	0.036	0.004	0.029				

Fig. 2 Influence of tool plunge depth during the welding process on the thermo-mechanical effect on the copper layer of a bimetallic sheet, **a** $d_t = 2$ mm, not causing TMAZ interference with the copper layer, and **b** $d_t = 2.6$ mm causing TMAZ interference with the copper layer

the bimetallic sheet, the value of the plunge depth being assumed to be $d_t = 2$ mm. In order to verify possible phenomena occurring at the AlCu bimetal interface, tests were also carried out using a plunge depth with a value that would cause thermoplastic changes in the copper layer (Fig. 2b); hence, the second value of the plunge depth that was considered was $d_t = 2.6$ mm. In this work, the "small plunge depth"—SD means $d_t = 2$ mm—and "large plunge depth"—LD means $d_t = 2.6$ mm. On the basis of preliminary research and general experience to date, the tool rotational speed was assumed to be a constant value equal to $n = 3000$ rpm [40].

This paper presents the influence of four combinations of RFSSW welding process parameters on the mechanical and microstructural properties of the joints of sheets made of EN AW-6082-T6 aluminum alloy with AlCu bimetallic sheet. The parameters analyzed are presented schematically in Fig. 3. For each variant, five joints were made, four of which were tested for load-bearing capacity, while the fifth sample was intended for metallographic tests.

2.3 Load capacity testing

Shear tests for determining the load capacity of joints were conducted according to the EN ISO 14273 [41] standard.
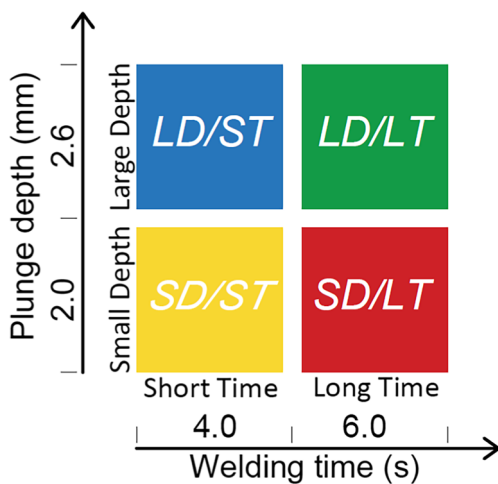

Fig. 3 Design matrix for the RFSSW parameters

Experiments were carried out at room temperature and a tensile speed of 5 mm/min. A Zwick/Roell Z100 was used as the testing machine. The single-lap specimens were attached to the grippers of the testing machine for a length of 30 mm.

2.4 Microstructural and fracture surface analysis

The morphology of the fracture surfaces of the welded joints was examined using an S-3400 Phenom ProX scanning electron microscope. Microstructure of selected specimens was analyzed using a S-3400N (Hitachi, Chiyoda, Japan) variable pressure scanning electron microscope (SEM). The samples were etched using Keller's solution (2 mL HF, 3 mL HCL, 5 mL HNO3, and 190 mL H2O). An analysis of the chemical composition was performed on selected areas of the microstructure in order to verify especially the phenomena occurring at the AlCu interface. The chemical composition analysis was conducted using energy dispersive spectrometry (EDS). Energy-dispersive X-ray (EDX) spectra were collected on the Quanta 3D 200i (FEI Company, Hillsboro, OR, USA) scanning electron microscope.

3 Results and discussion

### 3.1 Load capacity of RFSSW joints

The highest average value of the load capacity of the joint was demonstrated in the case of joints made with a tool plunge depth $d_t = 2.6$ mm and total welding time $t_w = 4$ s (LD/ST variant). The load capacity of the joint fabricated for this variant was on average 5986.75 N with a standard deviation equal to SD = 166.15 N (Table 2). As for the nature of the joint destruction observed on the macroscopic scale, in three out of four cases, the weld nugget was torn from the aluminum layer of the bimetallic sheet at the interface with the copper. This may indicate the influence of the TMAZ on the AlCu interface and the weakening of the material in this area, which will be subjected to a more detailed fractographic analysis presented in the next subsections.

Welding with a tool depth of $d_t = 2.6$ mm is related to the expansion of TMAZ toward the AlCu interface of the

Table 2 Analysis of failure modes and load capacity of RFSSW joints

Variant	Sample no	Failure mode	Load capacity, N	Average load capacity, N	Standard deviation of load capacity, N
LD/ST	1	nugget debonding	5803.33	5986.75	166.15
	2	plug type—Al layer_lower sheet	5977.47		
	3	plug type—Al layer_lower sheet	6253.58		
	4	plug type—Al layer_lower sheet	5912.61		
LD/LT	1	plug type – upper sheet	3856.48	4174.21	355.40
	2	plug type – upper sheet	4772.39		
	3	plug type – upper sheet	3974.22		
	4	plug type – upper sheet	4093.73		
SD/LT	1	nugget debonding	5868.45	5818.75	117.28
	2	nugget debonding	5957.16		
	3	nugget debonding	5636.11		
	4	nugget debonding	5813.29		
SD/ST	1	nugget debonding	5651.41	5442.26	179.21
	2	nugget debonding	5553.29		
	3	nugget debonding	5179.38		
	4	nugget debonding	5384.97		

bimetallic sheet. In this way, local degradation of the joint between the layers of the bimetallic sheet formed during roll bonding may occur. This is evidenced by the fact that in the majority of cases for the LD/ST variant, during strength tests, the Al bimetallic layer was torn off along the circumference of the weld. In this case, an important feature of the joint was also observed, i.e., based on the comparison of force–displacement curves (Fig. 4), it was found that the considered variant is characterized by the highest stiffness. This is undoubtedly related to the mechanism of destruction. In the case of the SD/LT and SD/ST variants, in the initial phase of the strength test, plastic deformation of the joint occurred due to the dominance of shear stresses. Then an increase in the bending moment occurs, as a result of which
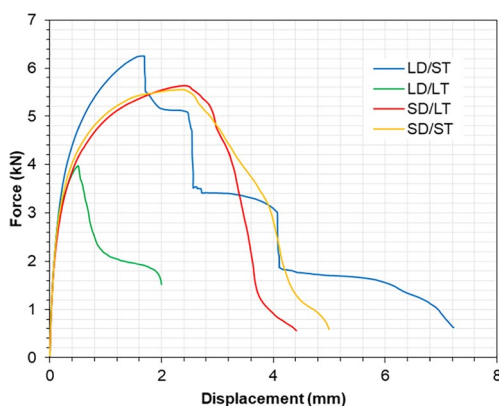
Fig. 4 Representative force–displacement curves for the variants of RFSSW joint that were evaluated
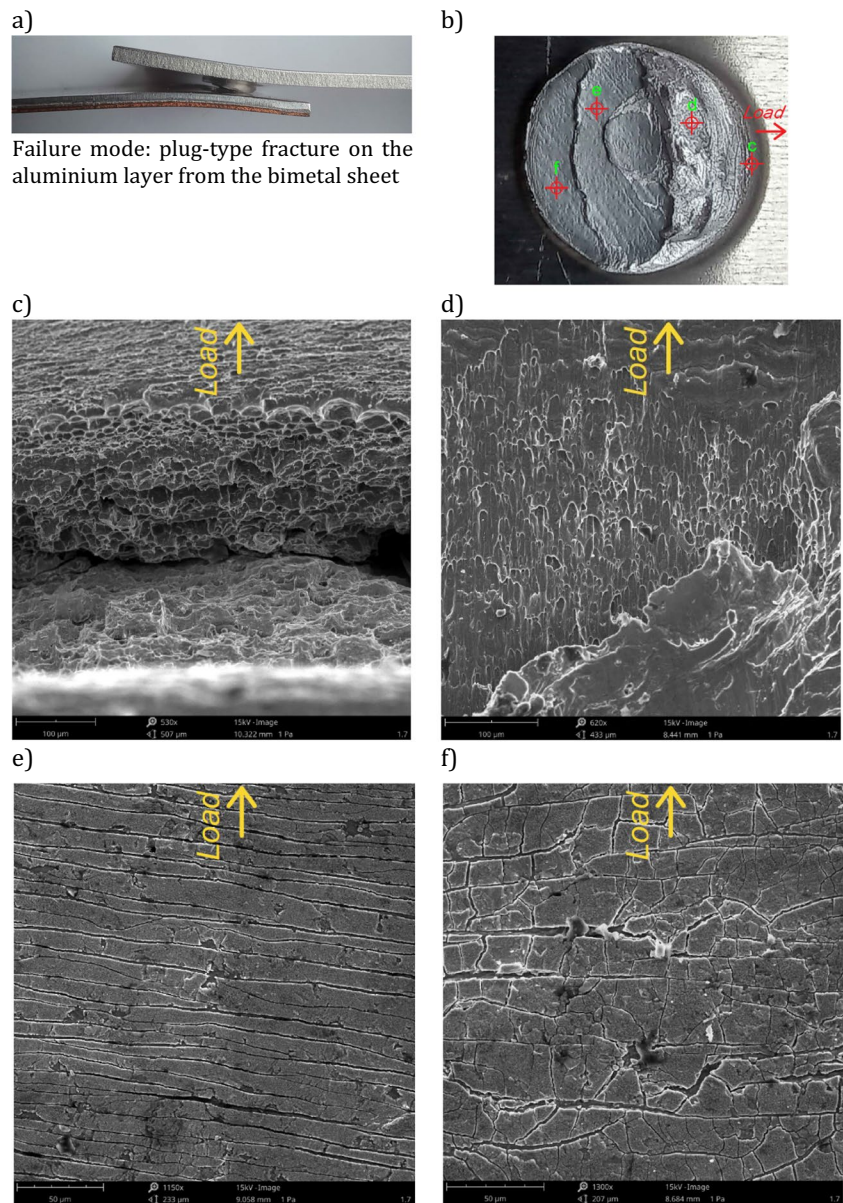
the joints failed due to the combined state of shear and peel stresses. The bending moment in the final phase of joint failure caused plastic deflection of the bimetallic sheet, which resulted in a decrease in joint stiffness.

A completely different character of the failure mechanism was observed for the LD/ST variant. Hypothetically, in most cases for this variant, the joint was shear loaded until the AlCu interface was broken, which was the first stage of joint destruction. Since the course of the force–displacement curve (Fig. 4) shows faults, it can be assumed that in the next stage, there was an increase in the value of the bending moment, which caused the plastic deflection of both sheets. Then circumferential cracking of the weld in the Al layer of the bimetallic sheet was observed, which finally resulted in breaking joint integrity.

The variants produced using tool plunge depth $d_t = 2$ mm have an almost identical character of stretch curves (Fig. 4). Macroscopic evaluation of the type of failure mode in each case showed the shear failure of the joints. However, joints produced using a longer welding time, i.e., $t_w = 6$ s, have a higher load capacity of 5818.75 N and, this should be emphasized, the highest degree of repeatability among all the variants considered with a standard deviation SD = 117.28 N (Table 2).

In the case of the plunge depth considered, the influence of the welding time on the load capacity of the joint is clearly visible. With a lower value of welding time, i.e., $t_w = 4$ s, there was a decrease in the average load capacity by 6.5% compared to the SD/LT variant, specifically to the value of 5442.26 N, while the standard deviation increased by 52.8% to the value of 179.21 N. Therefore,

Fig. 5 **a** View of the joint immediately after the shear test, **b** fracture surface on the upper sheet, **c–f** SEM fractographs of various fracture areas for a joint made using the welding time $t_w = 4$ s and tool plunge depth $d_t = 2.6$ mm (variant LD/ST)


a)

Failure mode: plug-type fracture on the aluminium layer from the bimetal sheet

b)

c)

d)

e)

f)

an insufficient amount of generated heat can be observed here at the welding time $t_w = 4$ s, which is a well-known phenomenon discussed by the authors of works on selecting the optimal parameters of the welding process when joining dissimilar materials [42–46]. Insufficient amount of heat does not allow proper thermomechanical phenomena to occur during welding, which usually results in a local lack of metallic continuity in the joint structure and other defects that affect not only the reduction of the joint's load capacity but also result in a greater dispersion of results. In this work, a limited range of parameters is presented for the purpose of preliminary recognition of their effect on the properties of the joint. However, further optimization studies are planned, in which each of the considered parameters will be considered at three levels as part of

the full factorial design of experiments (DoE). Then, the optimal value of the welding time will be indicated, after which excessive heat is generated. Excessive heat results in the weakening of the joint and excessive expansion of the HAZ, which has already been demonstrated in the case of joining other alloys [40].

The lowest load capacity, 4174.21 N, was noted for the LD/LT variant, and the greatest dispersion of the results was obtained with this case (SD = 355.40 N). With these parameters, the destruction of the joints was due to the pullout of the weld nugget from the upper sheet, which may indicate conditions in which there was insufficient joint welding, which translated into a poor connection of materials along the perimeter of the weld on the border of the TMAZ and the stir zone (SZ).

Fig. 6 Cross section of the RFSSW joint produced using welding time $t_w = 4$ s and tool plunge depth $d_t = 2.6$ mm (variant LD/ST) with visible IMC area
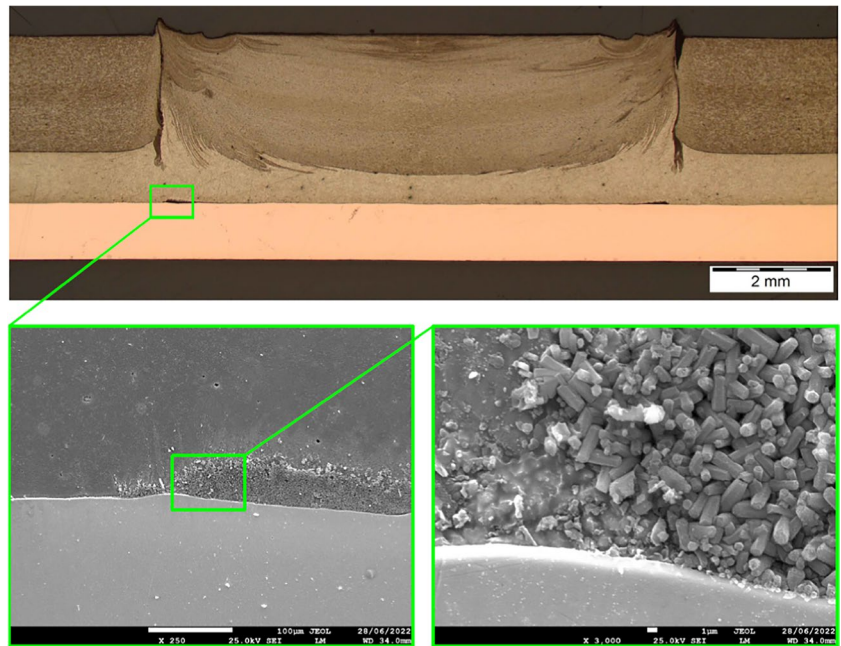
3.2 Fractographic analysis

3.2.1 LD/ST

In the case of the LD/ST variant, it was observed that the samples were repeatedly partially damaged by a plug-type fracture, i.e., the aluminum alloy layer was pulled out from the AlCu bimetallic sheet along the perimeter of the weld (Fig. 5a). The fracture surface on the side of the EN AW-6082-T6 aluminum alloy sheet is shown in Fig. 5b together with the areas of SEM analysis. The frontal joint area was subjected to plastic deformation, as evidenced by typical fractures for such a cracking mechanism with visible dimples (Fig. 5c). The shape of the dimples may indicate that in the initial phase of failure, normal stresses on the joint surface were dominant which caused the peel-off state. This is also shown by the deflection of the sheets due to the bending moment. A circumferential crack in the HAZ caused by the tensile stresses of the sheet can also be observed (Fig. 5c).

There were also areas observed on the fracture surface where the ductile failure occurred due to stresses tangential to the joint surface, as evidenced by the shape and arrangement of dimples (Fig. 5d). In the areas further away from the center of the weld nugget, surface fractures

Fig. 7 EDS linear scanning of the Al, Cu, and F element content in the transition zone between the Cu and Al layers of the bimetallic sheet
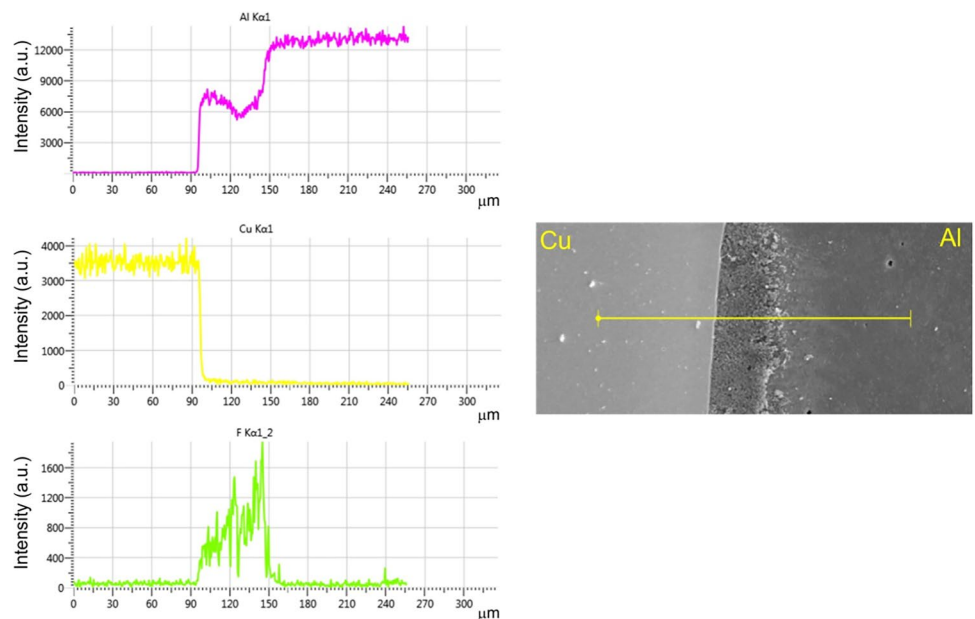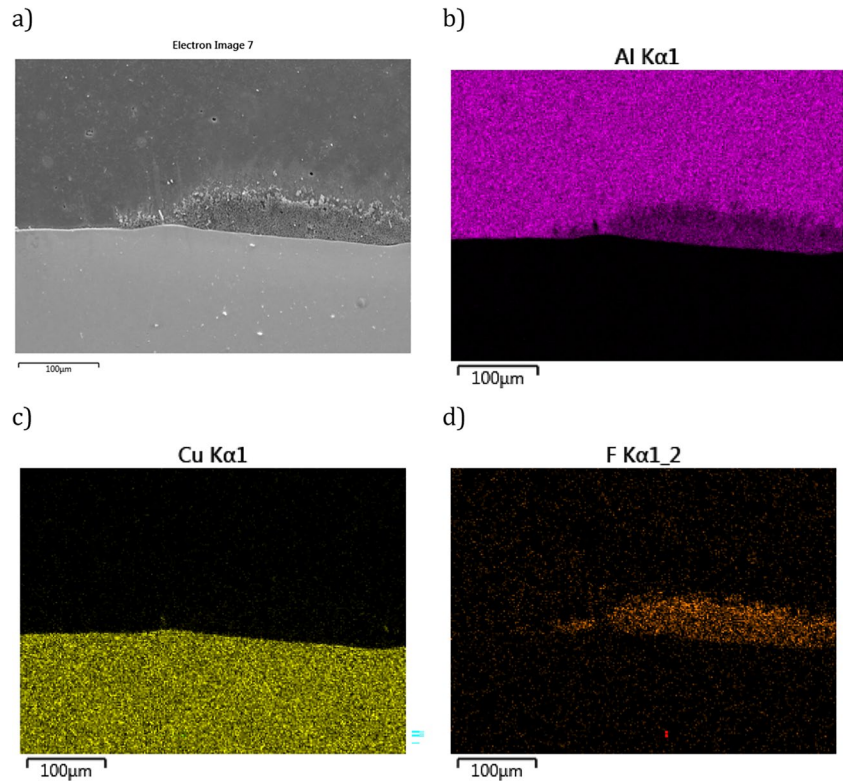
Fig. 8 a FESEM image and EDX elemental mapping of the interface area for the following elements: **b** Al, **c** Cu, and **d** F

are visible on the fracture surfaces (Fig. 5e, 5f). The plug height in the areas "e" and "f" in Fig. 5b is approximately 0.9 mm, so it is a level close to the interface between the bimetallic layers. The characteristic surface cracks may be the result of the impact of the tool generating thermo-mechanical processes during welding on the bimetal interface. The mechanical properties of the bimetallic sheet interface were formed during rolling, which locally led to strengthening, and thus made this region brittle.

The microstructure of the joint was analyzed in order to obtain more detail on the impact of pressure and friction produced by the tool during welding (Fig. 6). It was observed that there was an impact on the interface of the bimetallic sheet in the joint variant considered (LD/ST) which is visible on the marked area in the sleeve-affected zone in Fig. 6. As a result, a brittle intermetallic compound (IMC) was formed, which is disadvantageous for bimetallic sheets. IMCs weaken the interlayer bond, both in terms of static and fatigue strength. In the case of cyclic loads, IMCs occurring in a small area of the sleeve-affected zone can lead to the propagation of weakening and thus to local delamination of the bimetal. In addition, and this is important when using joints in electrotechnical systems, because of its flow characteristics IMCs cause a decrease in electrical and thermal conductivities. The IMC in the pin-affected zone was thicker than that in the sleeve-affected zone, a feature that has also been observed by Chai et al. [28].

This issue requires further experimental research to eliminate the phenomenon of the formation of IMC layers on the interface of the bimetallic sheet. It is extremely important to know the mechanisms of the formation of intermetallic phases and their causes. Abdollahzadeh et al. [47] carried out experimental studies and numerical finite element method analysis of the influence of selected welding parameters on the properties of FSSW aluminum-copper joints with an intermediate zinc layer. It was found that the change in shoulder diameter has a significant effect on the distribution and amount of heat generated during weld formation. Thermo-mechanical conditions during welding also have a significant impact on the grain size in the weld structure and the thickness of the intermetallic phases, which determines the directions of further research, which should largely concern the analysis of the amount and distribution of heat and its impact on the joint properties.

Vaneghi et al. [48] showed that the increase in rotational speed during and welding time in FSSW increases the amount of heat supplied to the bimetallic interface, which in turn leads to conditions that favor the formation of IMCs. In connection with the above-mentioned, an important optimization task arises aimed at selecting such parameters that would provide sufficient heat to form the correct joint, but at the same time, the development of IMC layers should be prevented.

Research should not be limited to the impact of welding process parameters on the formation of the considered

Fig. 9 a View of a plug type fracture on the upper sheet for a joint produced using the welding time $t_w = 6$ s and tool plunge depth $d_t = 2.6$ mm (variant LD/LT), **b** view of the fracture area on the upper and lower sheets, and **c–f** SEM fractographs of various fracture areas
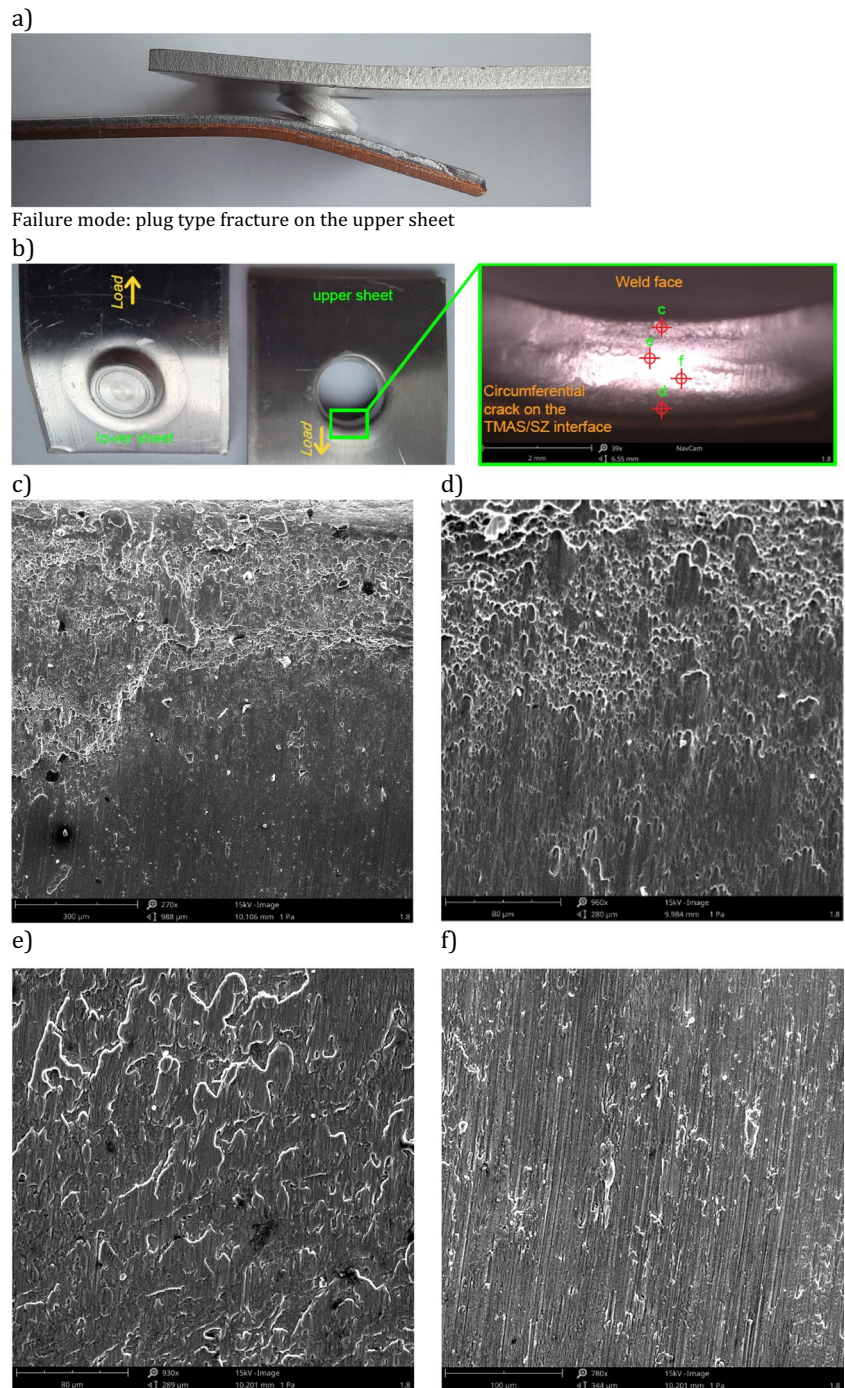
phenomenon because there are some tested ways of eliminating or at least significantly reducing the IMC layers. Abdollahzadeh et al. [49] conducted research on the impact of the nanoparticle interlayer used for FSSW welding sheets of aluminum alloy and copper. Using an intermediate layer made of SiC nanoparticles, the effect of this layer on IMC formation as well as other microstructure properties was studied. It has been shown that the use of a nanoparticle interlayer has a positive effect on the welded joint, leading to a reduction in the thickness of the IMC layer.

The transition zone between the copper and aluminum layers is weak due to the large difference in the chemical components of the roll-bonded sheets. As shown in Fig. 7,
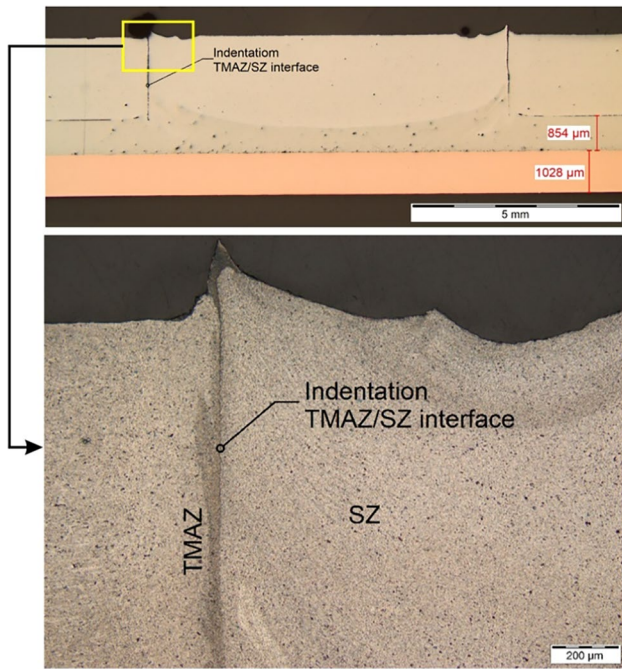
Fig. 10 Cross section of the RFSSW joint produced using welding time $t_w = 3$ s and tool plunge depth $d_t = 2.6$ mm

the width of the transition zone is approximately 60 μm. EDX elemental mapping of the interface area between the copper and aluminum layers is shown in Fig. 8.

3.2.2 LD/LT

In the case of the LD/LT joint variant, a plug-type fracture was repeatedly observed. Along its perimeter, the weld area was pulled out from the upper sheet (aluminum alloy) (Fig. 9a). When the SEM micrographs are analyzed, it can be seen that crack initiation took place from the upper plane of the sheet metal, where a plastic
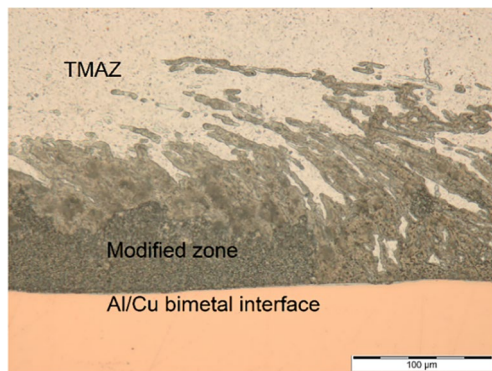
Fig. 11 Cross section of the interface of an EN AW-6082-T6 aluminum alloy/AlCu joint produced using the welding time $t_w = 3$ s and tool plunge depth $d_t = 2.6$ mm

fracture occurred, as evidenced by dimples (Fig. 9c). A similar phenomenon is visible on the lower plane of sheet metal (Fig. 9d). However, a completely different fracture was observed in the central area of the sheet thickness, where there are visible frictional traces of surface cooperation (Fig. 9e, 9f). The analysis of the joint microstructure indicates that a metallic connection may not have occurred locally in this area during the RFSSW process. This is confirmed by the discontinuity at the border between TMAZ and SZ, which is also the tool-sleeve interaction surface during welding (Fig. 10). These considerations lead to the conclusion that the combination of the adopted parameters, i.e., $t_w = 6$ s and $d_t = 2.6$ mm, does not provide the correct conditions for welding the joint. The structural discontinuity indicated along the TMAZ/SZ interface is a particularly unfavorable phenomenon from the point of view of cyclic loads causing fatigue.

Ensuring optimal thermo-mechanical conditions in order to produce the correct joint in terms of microstructure quality and strength is extremely important in friction stir welding processes. In this case, this issue requires consideration of a wider range of parameters and optimization analysis in future research. It is necessary to indicate such a correlation of the values of individual parameters of the welding process that would ensure the generation of the optimal amount of heat, i.e., sufficient to create a metallic joint in the entire weld area, but at the same time not leading to excessive growth of the heat affected zone, and undesirable direction of grain growth resulting in weakening of the joint. The essence of the problem is that each of the welding parameters affects the amount of heat generated. The rotational speed of the tool, due to the friction forces, generates heat in an amount proportional to the speed value. The amount of friction-generated heat increases with the welding time. In turn, plunge depth affects the heat dissipation area. Qiao et al. [50] analyzed how individual parameters affect the microstructure and the load capacity of RFSSW joints made of dissimilar metals, i.e., EN AW-6061 and 1Cr18Ni9Ti. At the same time, they indicated which aspects determine the quality of the joint, and that the selection of the right welding parameters requires optimization activities taking into account many criteria.

It is not only the parameters of the welding process that affect the properties of the welded joint microstructure. There is a possibility to stimulate the recrystallization, which is also worth considering in future research. Bagheri et al. [51] showed that the use of an intermediate layer of SiC nanoparticles at the interface of EN AW-5083 aluminum alloy sheets welded with copper sheets by the FSSW method

Fig. 12 EDS linear scanning of the Al, Cu, and F element content in the **a** transition and **b** modified zone between the Cu and Al layers of the bimetallic sheet
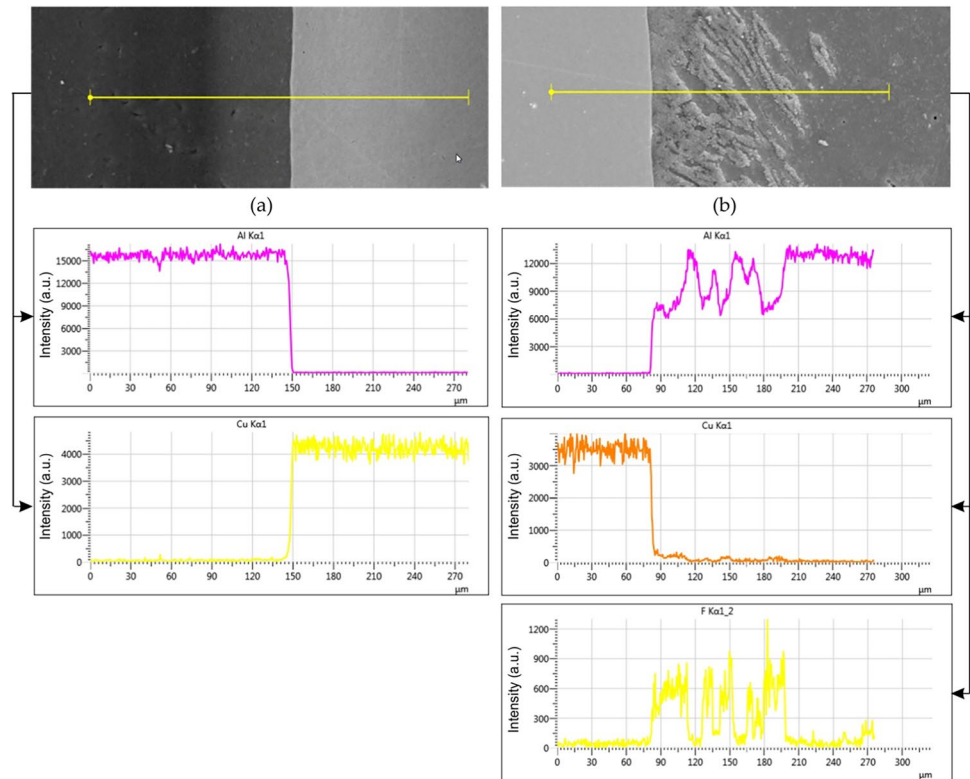
has a significant impact on the weld morphology. SiC nanoparticles are a factor influencing the course of the recrystallization process occurring during the welding of sheet metals.

This translates into the shape and size of grains in the joint microstructure, as well as the joint hardness and strength. Bagheri et al. [52] showed that the temperature distribution

Fig. 13 **a** FESEM image and EDX elemental mapping of the interface area for the following elements: **b** Al, **c** Cu, and **d** F
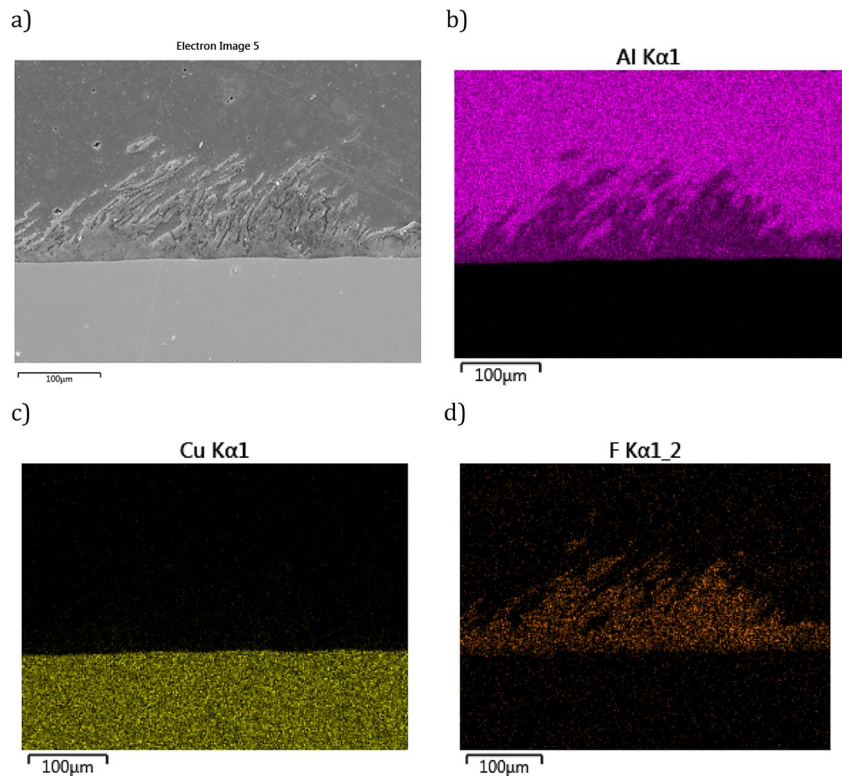
Fig. 14 EDS spectra of the interface of the bimetallic sheet (between the aluminum sheet and the copper sheet)
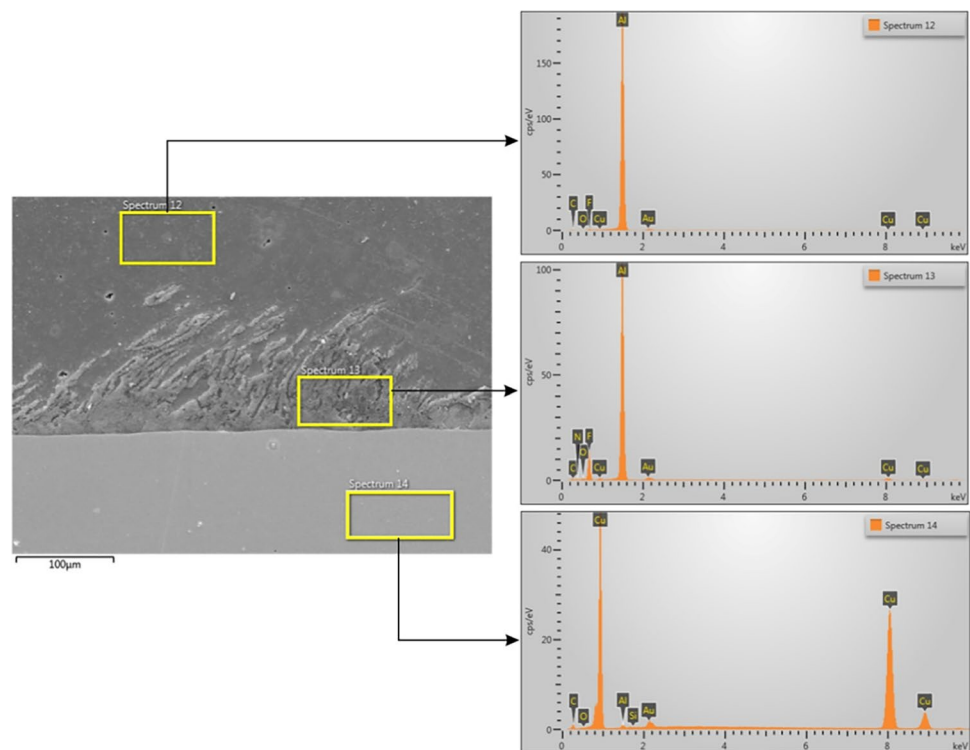
and the obtained grain sizes can be influenced by the size of SiC nanoparticles introduced as a layer between the welded sheets.

It is significant that a similar, although more intense, phenomenon of structural discontinuity was observed along the border between the TMAZ and SZ when performing preliminary welding tests using the time $t_w = 3$ s (Fig. 10). Such a variant was rejected as one of the preliminary tests based on the argument that too short a welding time does not ensure sufficient plasticization of the material to allow for the creation of structural continuity at the boundary of welded sheets. This may prove that there is a certain optimal value of the welding time in the interval between 3 and 6 s, which ensures that one obtains conditions under which the structural continuity of the joint is ensured.

As in the case of the previously described LD/ST variant, also in the case of tool depth $d_t = 2.6$ mm and of the LD/LT variant, there were significant changes in the bimetal interface which are shown in Fig. 11. However, for the LD/ST variant, the area of modified interface structure in the bimetal due to welding is greater than in the sleeve-affected zone alone, which proves a greater intensity of thermomechanical changes with increased welding time up to $t_w = 6$ s.

A comparative analysis of the chemical composition was performed by analyzing the bimetal interface outside the weld area (Fig. 12a). The individual transition phases were compared with the area (Figs. 12b and 13) in which phase changes were observed due to thermoplastic transformations occurring during the formation of the joint. The modified zone on the side of the aluminum sheet consists of a zone with a relatively high fluorine content. No increased copper content was observed in this zone. In the modified zone, a reduced content of aluminum was recorded compared to the content in the aluminum sheet included in the bimetallic sheet (Fig. 14). In addition, there is an increased content of fluoride in the modified area, which may indicate the occurrence of AlF_x [53].

The fluorine radicals may have been present as an impurity on the Al layer prior to the roll bonding process of the AlCu bimetallic sheet. This is a common phenomenon, e.g., when etching aluminum. These impurities during welding, as a result of the temperature and stresses acting during the formation of the weld, formed the aluminum fluoride areas, which are very unfavorable. These areas of aluminum fluoride contaminant cause intense oxidation of aluminum, which weakens the joint at the AlCu interface [54]. The local presence of this phenomenon was demonstrated in the area of pressure exerted by the sleeve during welding; however, this undesirable phenomenon under certain operating conditions could propagate, and in this way weaken the Al layer [55]. Therefore, there is a need to

Fig. 15 a View of the nugget debonding type fracture for a joint produced using the welding time $t_w = 6$ s and tool plunge depth $d_t = 2$ mm (variant SD/LT), **b** view of the fracture area on the upper sheet, and **c–f** SEM fractographs of various fracture areas


a)

Failure mode: nugget debonding

b)

c)

d)

e)

f)
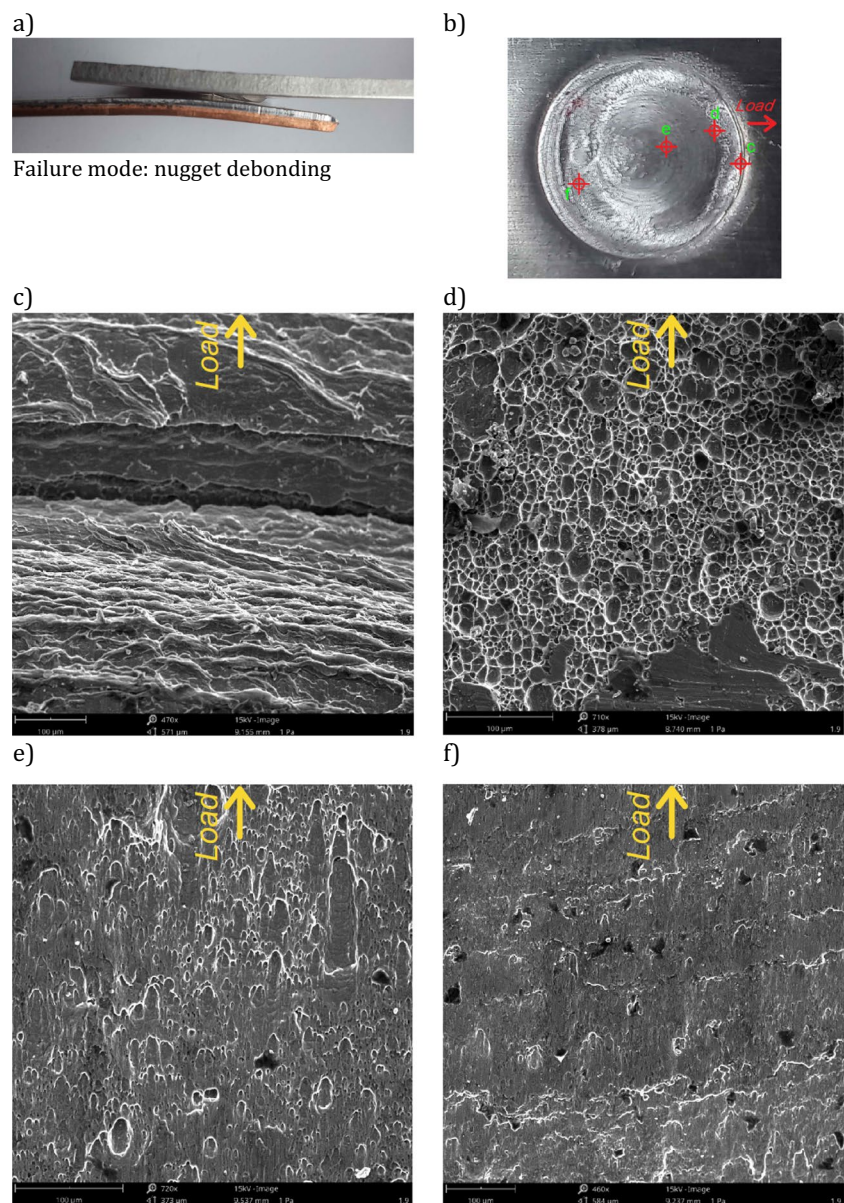
select parameters at which aluminum fluoride contaminant would not be formed.

3.2.3 SD/ST and SD/LT

In the case of joints fabricated with the use of a small tool plunge depth, i.e., $d_t = 2$ mm, a similar nature of failure was demonstrated, because in both variants (SD/ST and SD/LT) shear-type failure occurred in the joint plane (Fig. 15a). Figure 15b shows a fracture view on the upper sheet surface for a joint made using SD/LT parameters. In this figure, zones with different types of cracking can be observed. Figure 15c shows a view of a fracture at

the perimeter of the weld taken from the side where the load is applied. Moreover, a circumferential crack can be observed here as a result of the material weakening at the border of the SZ and TMAZ zones. In the area presented in Fig. 15d, one can observe dimples whose shape indicates a load direction perpendicular to the joint surface. This proves the local state of tearing off during the destruction of the joint, which is confirmed by the permanent deflection of both sheets due to the bending moment (Fig. 15a). In other areas of the joint fracture, ductile fracture typical to a shear type of fracture was observed. This is caused by tangential stresses on the joint surface (Fig. 15e, f).

Fig. 16 **a** View of the nugget debonding-type fracture for a joint produced using the welding time $t_w = 4$ s and tool plunge depth $d_t = 2$ mm (variant SD/ST), **b** view of the fracture area on the upper sheet, and **c–f** SEM fractographs of various fracture areas

Failure mode: nugget debonding
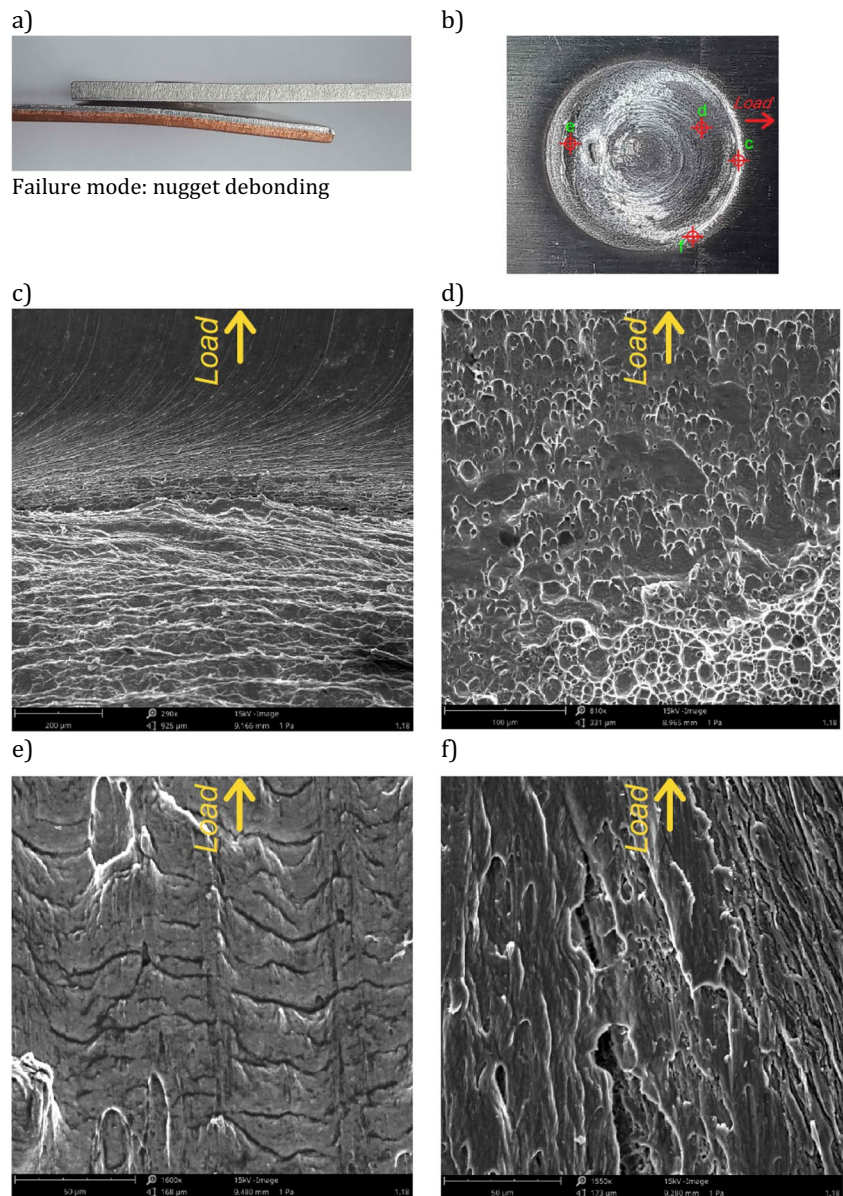
Although the character of failure of the joints corresponding to SD/ST is similar in general terms (Fig. 16a, b), some differences are noticeable. Namely, in this case, there was no circumferential fracture on the end face at the boundary between the TMAZ and SZ: see the sample load side in Fig. 16c. However, a similar crack was identified at the side edge of the joint in Fig. 16f.

In this case, the fracture areas that have been damaged by shear are dominant, and the fracture character is typically ductile (Fig. 16d, e). In this variant, the tangential stresses had a decisive influence on the mechanism of joint failure. This may also be proven by the fact that on a macroscopic scale, plastic deflection of the upper sheet was not observed. So, the values of bending moments causing normal stress, and thus the tear-out state, were significantly lower than in the case of the SD/LT joint variant.

4 Conclusions

In this article, the influence of welding parameters (tool plunge depth and welding time) on the strength of RFSSW joints of dissimilar materials was examined. On the basis of preliminary research, extreme values of input parameters were selected for which a welding process was performed. Based on the results, the following conclusions can be drawn:

1. The highest average value of the load capacity of the joint (5686.75 ± 166.15 N) was observed in joints made with a tool plunge depth $d_t = 2.6$ mm and total welding time $t_w = 4$ s.
2. The lowest load capacity of joints was recorded for the variant with the lowest tool depth $d_t = 2$ mm and shortest welding time $t_w = 4$ s examined. This load capacity was 4174.21 ± 355.4 N. The failure of the joint produced with these parameters was due to the pullout of the weld nugget from the upper sheet, which may indicate a poor connection of materials along the perimeter of the weld on the TMAZ/SZ interface.
3. Joints produced with a plunge depth of 2.6 mm were damaged by a plug-type fracture on the aluminum layer of the bimetallic sheet. Increasing the tool rotational speed and thus generating heat resulted in a plug-type fracture on the upper sheet (aluminum alloy).
4. In the case of joints produced with a plunge depth of 2 mm equal to the thickness of the upper sheet, the type of fracture mode with both welding times was found to be nugget debonding.
5. During welding sheets with a tool plunge depth of 2.6 mm, a zone of brittle IMCs was observed at the interface of the bimetallic sheets. IMCs are formed because of the heat input and flow of the base materials while subject to intense pressure. The location of the IMCs' zone depends on the welding conditions. During welding according to the LD/ST variant, the area of modified interface microstructure in the bimetal due to welding is larger than that solely in the sleeve impact area (LD/LT variant), which proves that there is a greater intensity of thermo-mechanical change as welding time increases from $t_w = 4$ s to $t_w = 6$ s.

Declarations

Ethical approval The authors declare the compliance with the ethical standards.

Consent to participate Not applicable.

Consent for publication Not applicable.

Conflict of interest The authors declare no competing interests.

References

1. Sahu PK, Pal S, Pal SK, Jain R (2016) Influence of plate position, tool offset and tool rotational speed on mechanical properties and microstructures of dissimilar Al/Cu friction stir welding joints. J Mater Process Technol. https://doi.org/10.1016/j.jmatprotec.2016.04.014
2. Zhang JP, Huang HG, Sun JN, Zhao RD, Feng M (2022) Interfacial pressure distribution and bonding characteristics in twin-roll casting of Cu/Al clad strip. Trans Nonferrous Met Soc China. https://doi.org/10.1016/S1003-6326(22)65996-X
3. Kocich R, Macháčková A, Kuncická L, Fojtík F (2015) Fabrication and characterization of cold-swaged multilayered Al–Cu clad composites. Mater Des. https://doi.org/10.1016/j.matdes.2015.01.008
4. Li XB, Zu GY, Wang P (2015) Microstructural development and its effects on mechanical properties of Al/Cu laminated composite. Trans Nonferrous Met Soc China. https://doi.org/10.1016/S1003-6326(15)63576-2
5. Francis R (2017) Galvanic corrosion: a practical guide for engineers, second edition. NACE Int
6. Jandaghi MR, Saboori A, Khalaj G, KhanzadehGharehShiran M (2020) Microstructural evolutions and its impact on the corrosion behaviour of explosively welded Al/Cu bimetal. Metals. https://doi.org/10.3390/met10050634
7. Zhang LF, Gao R, Zhao BL, Sun M, Jing K, Wang XP, Hao T, Xie ZM, Liu R, Fang QF, Liu CS (2020) Effects of annealing temperature and layer thickness on hardening behavior in cross accumulative roll bonded Cu/Fe nanolamellar composite. J Alloys Compd. https://doi.org/10.1016/j.jallcom.2020.154312
8. Sun Y, Rong Z, Guan S (2020) Surface solid-state amorphization of accumulative roll bonded Cu-Zr laminates by friction stir processing. Mater Lett. https://doi.org/10.1016/j.matlet.2020.128518
9. Uscinowicz R (2013) The effect of rolling direction on the creep process of Al–Cu bimetallic sheet. Mater Des. https://doi.org/10.1016/j.matdes.2013.02.012
10. Wang J, Zhao F, Xie G, Hou Y, Wang R, Liu X (2021) Rolling deformation behaviour and interface evaluation of Cu-Al bimetallic composite plates fabricated by horizontal continuous

composite casting. J Mater Process Technol. https://doi.org/10.1016/j.jmatprotec.2021.117296

11. Chekhonin P, Zöllner D, Zimmer E, Scharnweber J, Romberg J, Skrotzki W (2019) Microstructure of accumulative roll bonded high purity aluminium laminates. Materialia. https://doi.org/10.1016/j.mtla.2019.100236

12. McCabe RJ, Nizolek TJ, Li N, Zhang Y, Coughlin DR, Miller C, Carpenter JS (2021) Evolution of microstructures and properties leading to layer instabilities during accumulative roll bonding of FeCu, FeAg, and FeAl. Mater Des. https://doi.org/10.1016/j.matdes.2021.110204

13. Morovvati MR, Mollaei-Dariani B, Asadian-Ardakani MH (2013) A theoretical, numerical, and experimental investigation of plastic wrinkling of circular two-layer sheet metal in the deep drawing. J Mater Process Technol. https://doi.org/10.1016/j.jmatprotec.2010.06.004

14. Jiang W, Guan F, Li G, Jiang H, Zhu J, Fan Z (2019) Processing of Al/Cu bimetal via a novel compound casting method. Mater Manu Proc 34:1016–1025

15. Ólafsson DI (2017) Friction stir welding of aluminium - copper. MSc Thesis. Aalto University, Aalto

16. Galvão I, Leal R, Loureiro A, Rodrigues D (2010) Material flow in heterogeneous friction stir welding of aluminium and copper thin sheets. Sci Technol Weld Join. https://doi.org/10.1179/136217110X1278588955010

17. Bhattacharya TK, Das H, Jana SS, Pal TK (2017) Numerical and experimental investigation of thermal history, material flow and mechanical properties of friction stir welded aluminium alloy to DHP copper dissimilar joint. Int J Adv Manuf Technol. https://doi.org/10.1007/s00170-016-8820-0

18. Liu HJ, Shen JJ, Xie S, Huang YX, Cui F, Liu C, Kuang LY (2012) Weld appearance and microstructural characteristics of friction stir butt barrier welded joints of aluminium alloy to copper. Sci Technol Weld Join. https://doi.org/10.1179/1362171811Y.0000000086

19. Galvão I, Oliveira J, Loureiro A, Rodrigues D (2011) Formation and distribution of brittle structures in friction stir welding of aluminium and copper: Influence of process parameters. Sci Technol Weld Join. https://doi.org/10.1179/1362171811Y.0000000057

20. Galvão I, Loureiro A (2015) Rodrigues DM (2016) Critical review on friction stir welding of aluminium to copper. Sci Technol Weld Join. https://doi.org/10.1080/13621718.1118813

21. Barekatain H, Kazeminezhad M, Kokabi A (2014) Microstructure and Mechanical properties in dissimilar butt friction stir welding of severely plastic deformed aluminum AA 1050 and commercially pure copper sheets. J Mater Sci Technol. https://doi.org/10.1016/j.jmst.2013.11.007

22. Manickam S, Rajendran C, Balasubramanian V (2020) Investigation of FSSW parameters on shear fracture load of AA6061 and copper alloy joints. Heliyon. https://doi.org/10.1016/j.heliyon.2020.e04077

23. Balasubramanian V (2008) Relationship between base metal properties and friction stir welding process parameters. Mater Sci Eng A. https://doi.org/10.1016/j.msea.2007.07.048

24 Gadakh VS, Badheka VJ, Mulay AS (2021) Solid-state joining of aluminum to titanium: a review. Proc Inst Mech Eng, Part L: J Mater: Des Appl. https://doi.org/10.1177/14644207211010839

25. Chowdhury SH, Chen DL, Bhole SD, Cao X, Wanjara P (2013) Lap shear strength and fatigue behavior of friction stir spot welded dissimilar magnesium-to-aluminum joints with adhesive. Mater Sci Eng A. https://doi.org/10.1016/j.msea.2012.11.039

26. Suhuddin UFH, Fischer V, dos Santos JF (2013) The thermal cycle during the dissimilar friction spot welding of aluminum and magnesium alloy. Scripta Mater. https://doi.org/10.1016/j.scriptamat.2012.09.008

27. Elyasi M, Taherian J, Hosseinzadeh M, Kubit A, Aghajani DH (2023) The effect of pin thread on material flow and mechanical properties in friction stir welding of AA6068 and pure copper. Heliyon. https://doi.org/10.1016/j.heliyon.2023.e14752

28. Chai P, Hu W, Ji S, Ai X, Lv Z, Song Q (2019) Refill friction stir spot welding dissimilar Al/Mg alloys. J Mater Eng Perform. https://doi.org/10.1007/s11665-019-04359-7

29. Zou Y, Li W, Yang X, Patel V, Shen Z et al (2022) Characterizations of dissimilar refill friction stir spot welding 2219 aluminum alloy joints of unequal thickness. J Manuf Process. https://doi.org/10.1016/j.jmapro.2022.04.062

30. Liu Z, Yang K, Yan D (2019) Refill friction stir spot welding of dissimilar 6061/7075 aluminum alloy. High Temp Mater Process. https://doi.org/10.1515/htmp-2017-0139

31. Fritsche S, Draper J, Toumpis A, Galloway A, Amancio-Filho ST (2022) Dissimilar joints of additive manufactured and wrought aluminium alloy produced by refill friction stir spot welding. Poster session presented at Advanced Materials Poster Day.; Graz, Austria

32. Kubit A, Trzepieciński T, Gadalińska E, Slota J, Bochnowski W (2021) Investigation into the effect of RFSSW parameters on tensile shear fracture load of 7075–T6 Alclad aluminium alloy joints. Materials. https://doi.org/10.3390/ma14123397

33. Kubit A, Faes K, Jurczak W, Bucior M, Kluz R (2020) Analysis of the properties of RFSSW lap joints of Alclad 7075-T6 aluminum alloy sheets under static and dynamic loads. Technol Automat Mont. https://doi.org/10.15199/160.2020.4.1

34. Takeoka N, Tsuchida T, Matsuda T, Ogura T, Ohashi R, Hirose A (2022) Analysis of mechanical properties of dissimilar material joint using scrubbing refill friction stir spot welding. J Adv Join Process. https://doi.org/10.1016/j.jajp.2022.100112

35. Nunes R, Faes K, De Meester S, De Waele W, Kubit A (2022) Influence of welding parameters and surface preparation on thin copper–copper sheets welded by ultrasonic welding process. Int J Adv Manuf Technol. https://doi.org/10.1007/s00170-022-10164-9

36. Pati PR, Das S, Satpathy MP, Routara BC, Sahoo SK, Bhuyan SK (2020) Ultrasonic spot welding of Al-Cu sheets: a comprehensive study. Mater Today Proc. https://doi.org/10.1016/j.matpr.2020.02.873

37. Das A, Barai A, Masters I, Williams D (2019) Comparison of tab-to-busbar ultrasonic joints for electric vehicle Li-ion battery applications. World Electr Veh J. https://doi.org/10.3390/wevj10030055

38. Lee SS, Kim TH, Hu SJ, Cai WW, Abell JA, Li J (2013) Characterization of joint quality in ultrasonic welding of battery tabs. J Manuf Sci Eng 2013. https://doi.org/10.1115/1.4023364

39. Zhang LF, Gao R, Zhao BL, Sun M, Jing K, Wang XP, Hao T, Xie ZM, Liu R, Fang QF et al (2020) Effects of annealing temperature and layer thickness on hardening behavior in cross accumulative roll bonded Cu/Fe nanolamellar composite. J Alloys Compd. https://doi.org/10.1016/j.jallcom.2020.154312

40. Kluz R, Kubit A, Trzepiecinski T, Faes K, Bochnowski W (2019) A Weighting grade-based optimization method for determining refill friction stir spot welding process parameters. J Mater Eng Perform. https://doi.org/10.1007/s11665-019-04378-4

41. EN ISO 14273 (2000) Specimen dimensions and procedure for shear testing resistance spot, seam and embossed projection welds; International Organization for Standardization: Geneva, Switzerland

42. Al-Zubaidy BMM (2016) Material interactions in a novel refill friction stir spot welding approach to joining Al-Al and Al-Mg automotive sheets. Ph.D. Thesis, University of Menchester, Menchester, UK

43. Schmal C, Meschut G, Buhl N (2019) Joining of high strength aluminum alloys by refill friction stir spot welding (III-1854-18). Weld World. https://doi.org/10.1007/s40194-018-00690-0

44. Nadan R, Roy GG, Lienert TJ, Debroy T (2007) Three-dimensional heat and material flow during friction stir welding of mild steel. Acta Mater. https://doi.org/10.1016/j.actamat.2006.09.009

45. Uematsu Y, Tokaji K, Tozaki Y, Kurita T, Murata S (2008) Effect of re-filling probe hole on tensile failure and fatigue behaviour of friction stir spot welded joints in Al–Mg–Si alloy. Int J Fatigue. https://doi.org/10.1016/j.ijfatigue.2008.01.006

46. Zhao YQ, Liu HJ, Chen SX, Lin Z, Hou JC (2014) Effects of sleeve plunge depth on microstructures and mechanical properties of friction spot welded alclad 7B04-T74 aluminum alloy. Mater Des. https://doi.org/10.1016/j.matdes.2014.05.012

47. Abdollahzadeh A, Bagheri B, Vaneghi AH, Shamsipur A, Mirsalehi SE (2022) Advances in simulation and experimental study on intermetallic formation and thermomechanical evolution of Al–Cu composite with Zn interlayer: effect of spot pass and shoulder diameter during the pinless friction stir spot welding process. Proc Inst Mech Eng, Part L: J Mater Des Applic https://doi.org/10.1177/14644207221146981

48. Vaneghi AH, Bagheri B, Shamsipur A, Abdollahzadeh A (2022) Investigations into the formation of intermetallic compounds during pinless friction stir spot welding of AA2024-Zn-pure copper dissimilar joints. Weld World. https://doi.org/10.1007/s40194-022-01366-6

49. Abdollahzadeh B, Bagheri B (2022) Shamsipur A (2022) Development of Al/Cu/SiC bimetallic nano-composite by friction stir spot welding. Mater Manuf Proc. https://doi.org/10.1080/10426914.2157435

50. Qiao F, Cheng K, Wang L, Guo L (2016) An experimental investigation on the dissimilar joining of AA6061 and 1Cr18Ni9Ti by refill friction stir spot welding and its mechanical properties. Proc Inst Mech Eng, Part B: J Eng Manuf. https://doi.org/10.1177/0954405415603599

51. Bagheri B, Abdollahzadeh B, Shamsipur A (2023) A different attempt to analysis friction stir spot welding of AA5083-copper alloys. Mater Sci Tech. https://doi.org/10.1080/02670836.2022.2159633

52. Bagheri B, Shamsipur A, Abdollahzadeh A, Mirsalehi SE (2023) Investigation of SiC nanoparticle size and distribution effects on microstructure and mechanical properties of Al/SiC/Cu composite during the FSSW process: experimental and simulation. Met Mater Int. https://doi.org/10.1007/s12540-022-01284-8

53. Ernst KH, Grman D, Hauert R, Holländer E (1994) Fluorine-induced corrosion of aluminium microchip bond pads: an XPS and AES analysis. Surf Interf Anal. https://doi.org/10.1002/sia.740211003

54. Kim MS, Lee JW (2020) Effect of seasoning-layer stress on fluorine diffusion. AIP Adv. https://doi.org/10.1063/5.0015318

55. Fan C, Yin N, Cai X, Du X, Wang P, Liu X, Li Y, Chang X, Du H, Ma J, Cui Y (2022) Stabilization of fluorine-contaminated soil in aluminum smelting site with biochar loaded iron-lanthanide and aluminum-lanthanide bimetallic materials. J of Haz Mat. https://doi.org/10.1016/j.jhazmat.2021.128072